# Angle-Resolved X-ray Photoelectron Spectroscopy of in Situ Deposited Li on $MoS_2(0002)$†

**Ken T. Park,*,‡ Jie Kong,‡ and Kamil Klier*,§**

*Department of Physics, Baylor University, Waco, Texas 76798, and Department of Chemistry and Zettlemoyer Center for Surface Studies, Lehigh University, Bethlehem, Pennsylvania 18015*

*Received: September 15, 1999; In Final Form: December 10, 1999*

A contrasting behavior in alkali/$MoS_2$ composites is demonstrated between a reductive reconstruction in the Li/$MoS_2$ system and previously reported pure electron transfer in Cs/$MoS_2$. The interaction of in situ cleaved 2H−$MoS_2$(0002) with Li was investigated using angle-resolved X-ray photoelectron spectroscopy (ARXPS). The high-resolution XPS in the core level regions revealed that the deposited Li reduced $MoS_2$(0002) into $Li_2S$/Mo(II)S via the reaction $2Li + MoS_2 \rightarrow Li_2S + MoS$, evidenced by the binding energies and the stoichiometry of Mo, S, and Li. The ARXPS data of the Li 1s, Mo 3d, and S 2p core levels further indicated that the deposited Li together with the reduced $MoS_2$ surface formed a highly disordered surface region, which extended approximately 12 Å deep into the $MoS_2$ bulk. The valence band XPS also revealed a clearly different interaction of Li with $MoS_2$ from that of Cs. The supravalence electron density of states in Li/$MoS_2$ appeared at ca. 0.3 eV above the $MoS_2$ valence band maximum (VBM), whereas that from Cs/$MoS_2$ was previously observed at 1.25 eV above the VBM, very close to the conduction band minimum of $MoS_2$. Thus, the interaction of Li with $MoS_2$ cannot be characterized by a rigid band model unlike that which made a good approximation for the Cs/$MoS_2$ system. The Li/$MoS_2$ specimens were also exposed to molecular oxygen, and the formation of surface peroxide is reported herein.

## Introduction

Molybdenum disulfide ($MoS_2$) belongs to a family of materials called layered transition metal dichalcogenides. It possesses a highly anisotropic structure in which covalently bonded chalcogen−metal−chalcogen atom sheet sandwiches are loosely coupled via van der Waals interactions (Figure 1).[1] Within each $MoS_2$ layer, a molybdenum atom is surrounded by six nearest-neighbor sulfur atoms in trigonal prismatic coordination. The highly anisotropic structure of $MoS_2$ gives rise to interesting mechanical, electrical, optical, tribological, and catalytic properties. In particular, the interaction of $MoS_2$ with alkali metals has been the subject of a number of studies. Earlier studies focused on understanding the superconductivity of alkali metal intercalated $MoS_2$.[2−4] Other studies demonstrated the application of Li-doped $MoS_2$ as an energy-storing device.[5−7] It was also reported that alkali metal could play an important role as a surface promoter for catalytic synthesis of alcohols from carbon monoxide and hydrogen gas over $MoS_2$.[8−11]

All of the applications mentioned above involve charge transfer from alkali metal atoms to the $MoS_2$. Therefore, the investigation of elementary electron-transfer processes taking places on $MoS_2$ surfaces and understanding of the fundamental mechanism that governs the electron transfer reactions are highly desirable. In an attempt to achieve sound understanding of the surface atomic and electronic structures, the steps involved in electron transfer, and the nature of surface bonding on a well-defined single crystal surface, we have previously investigated the adsorption of Cs with $MoS_2$(0002) surface using HRXPS.[12−14] In that study, we reported that Cs adatoms formed a disordered overlayer without inducing any structural modification of the $MoS_2$ surface.[12] The adsorption of Cs onto the basal plane gave rise to a new density of states ca. 1.25 eV above the valence band (VB) maximum of a bare $MoS_2$(0002) (the "supravalence electronic state").[13] Theory and angle-resolved X-ray photoelectron spectroscopy (ARXPS) of this newly occupied state indicated that the new VB states originated mainly from the bottom of the conduction band (CB) of a bare $MoS_2$ mixed to a small extent with the Cs 6s state, suggesting an electron transfer to the substrate similar to that described by a rigid band model. Furthermore, we have recently demonstrated that the supravalence electrons in $MoS_2$ could be captured and react with electron acceptor molecules such as molecular chlorine, oxygen, and water to form surface chloride, peroxide, superoxide, and hydroxide species.[14] In an investigation of the opposite end-member of the alkali series, Papageorgopoulos and Jaegermann studied the composite of Li with $MoS_2$,[15] with Li as the lightest alkali metal on the chalcogenide.[16] These authors reported that at room-temperature deposition, Li intercalated into $MoS_2$ forming $Li_xMoS_2$ at low Li coverage ($0 < x < 0.2$), but at high values of $x$, the intercalation reaction was accompanied by the 2H to 1T phase transition. The authors further concluded that the observed charge transfer and the subsequent phase transition could be interpreted in terms of a rigid band model. The dramatically different behavior of Cs and Li on $MoS_2$(0002) surface motivated us to re-examine the similarities and differences in surface chemistry involving the two alkali metals. In this paper, we present a study of the Li adsorption on a $MoS_2$-(0002) surface using angle-resolved X-ray photoelectron spectroscopy (ARXPS). ARXPS is chosen as a powerful surface diagnostic tool to render short-range local, atomic structure of a near-surface region along with an element-specific and chemical-state-specific electronic information. Especially for

† Part of the special issue "Gabor Somorjai Festschrift".
‡ Baylor University.
§ Lehigh University.

10.1021/jp993298s CCC: $19.00 
Published on Web 02/02/2000

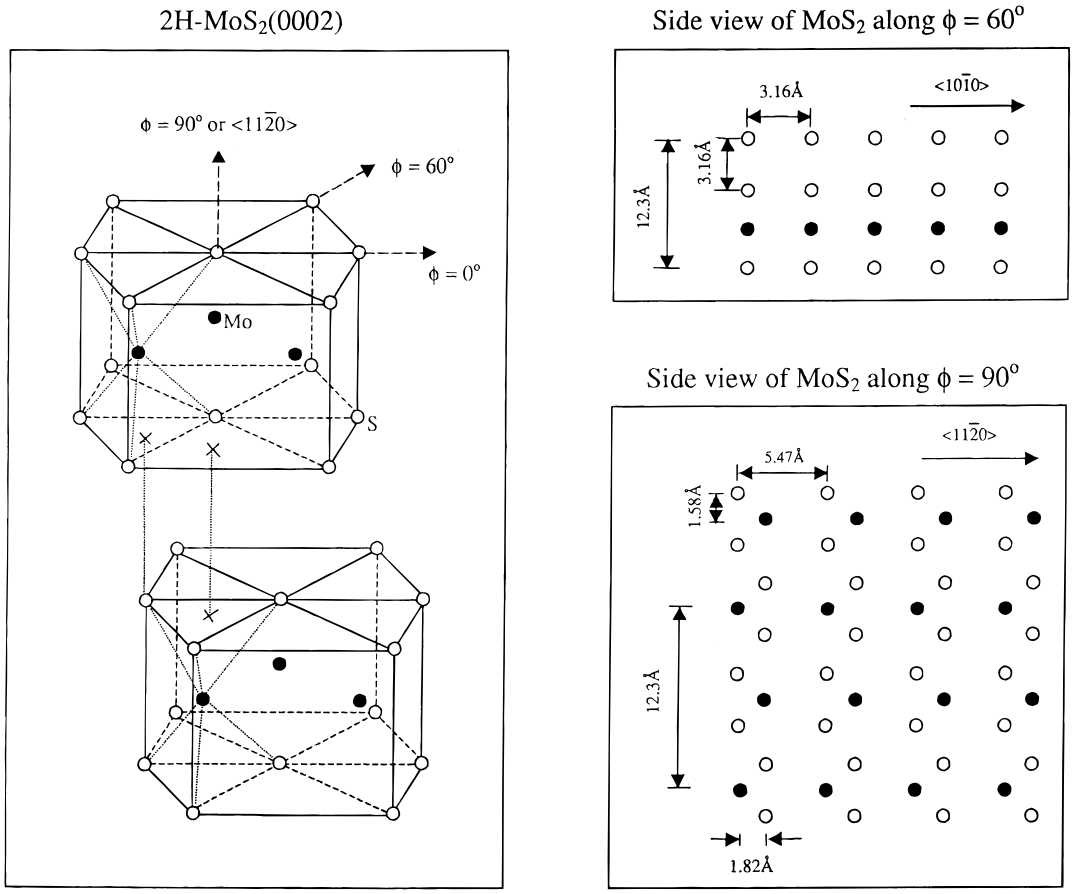


**Figure 1.** Three-dimensional view of the 2H−$MoS_2$ structure (left). Also presented are cross-sectional views of a single-crystal $MoS_2$ (0002) surface along $\phi = 60°$ (top right panel) and along $\phi = 90°$ (bottom right panel).

X-ray photoelectrons of kinetic energy above 500 eV, strong intensity maxima are observed on single crystals along directions connecting a subsurface emitter atom with scatterer atoms in the path of escaping photoelectrons.[17,18] These intensity variations known as forward-projected images of the top few surface layers make the interpretation of the ARXPS data relatively simple and consequently make ARXPS a valuable structural tool.[12] Thus, the core-level ARXPS data from Li/$MoS_2$ could provide direct evidence of the proposed 2H to 1T phase transition particularly via X-ray photoelectron diffraction (XPD) dominated by forward focusing. In the valence band (VB) region, the ARXPS data could provide the VB spectra of the Li-deposited $MoS_2$(0002) integrated over the Brillouin zone[19] as a complementary information to the ultraviolet photoemission spectroscopy (UPS) data obtained by Papageorgopoulos and Jaegermann and at the same time allow us to directly compare the VB XPS spectra of the Li/$MoS_2$(0002) and Cs/$MoS_2$(0002).

## Experimental Section

The experiments were carried out in an ultrahigh vacuum system, which accommodates the SCIENTA ESCA-300 HRXPS spectrometer. The SCIENTA ESCA-300 HRXPS spectrometer uses its uniquely designed, water-cooled rotating anode to produce high-intensity X-ray beam at Al Kα line ($h\nu = 1486.8$ eV). The high-power X-ray beam (up to ca. 8 kW) is then monochromatized by seven individually adjustable, toroidally bent quartz crystals, and the photoemitted electrons are detected using a 300 mm mean radius hemispherical energy analyzer. The samples are positioned at the focal point of the spectrometer using the high precision, automated sample manipulator/goniometer (Seiko Instruments), which allows three degrees of translational motion as well as two degrees of rotational motion. For ARXPS experiments, the sample is aligned to ⟨10$\bar{1}$0⟩ crystallographic direction using the well-documented positions of the forward focusing maxima of pure $MoS_2$. The polar angle XPS scans are then obtained at 1° increments from −3° to 67° measured from the surface normal. Detailed information on the sample geometry and the SCIENTA ESCA-300 HRXPS spectrometer are available elsewhere.[20,21]

All the $MoS_2$ (0002) single crystals studied in the experiments were in the form of the natural mineral molybdenite, obtained from Ward's Natural Science Establishment. A clean well-ordered surface of $MoS_2$ (0002) was obtained by in situ peeling off the top surface layers in the ultrahigh vacuum (UHV) system, using double sided adhesive tape on each peeled piece. This method of in situ cleaving has proven to produce a clean well-ordered basal plane of $MoS_2$ as evidenced by XPS and low-energy electron diffraction (LEED) pattern with low background intensity using a reverse view LEED optics (Princeton Instrument RVL 8-120).[12−14] Lithium was deposited onto the basal plane of $MoS_2$ at room temperature using a commercial Li getter source (SAES). Prior to deposition, the Li source in the preparation chamber was thoroughly degassed to minimize the possibility of coadsorbing ambient gases during the evaporation. The Li evaporation time was gradually incremented from 0 to 10, 25, 55, 115, and 195 min. For studying the interaction of Li/$MoS_2$ (0002) with $O_2$, the of Li/$MoS_2$ (0002) surface was exposed to oxygen gas at room temperature. The initial exposure of $1.8 \times 10^3$ L of $O_2$ ($P_{O_2} = 10^{-6}$ Torr for 30 min) was carried

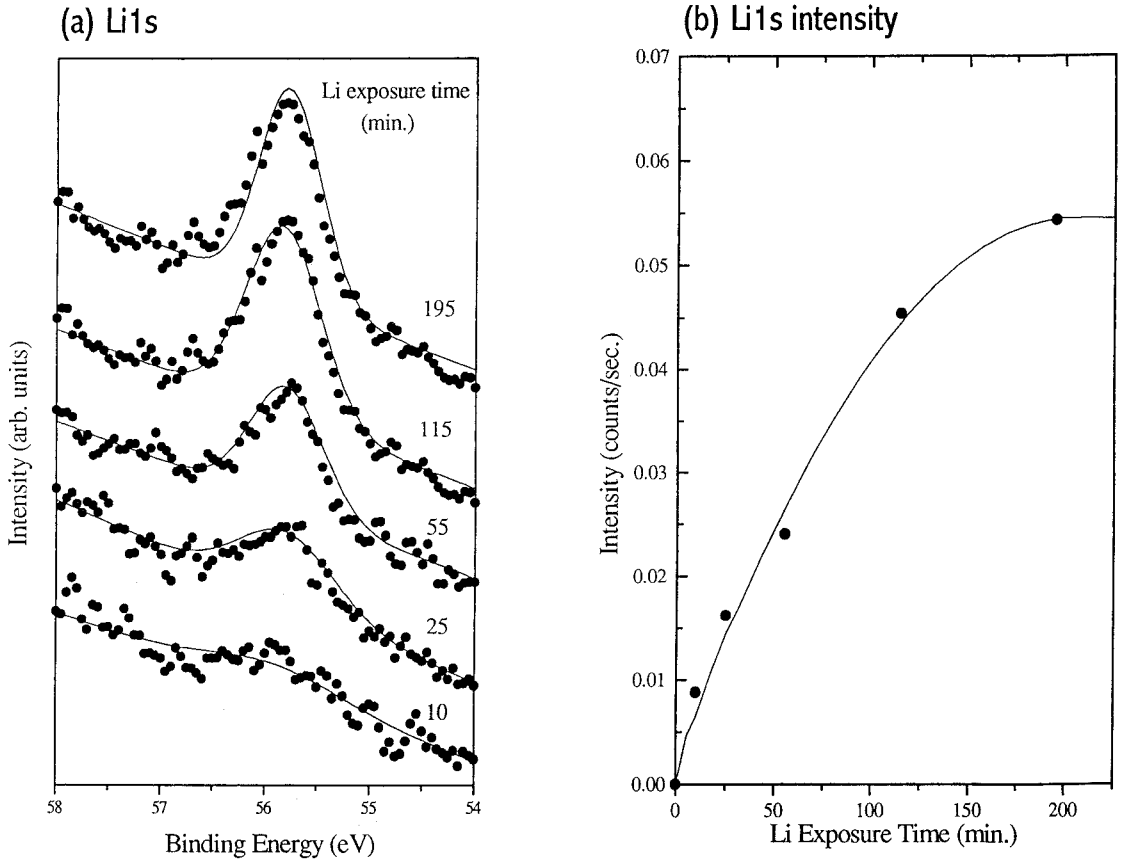


**Figure 2.** The effect of Li deposition on Li 1s peak. (a) Li 1s peak at different Li exposure time. (b) The intensity of Li 1s peak (peak area) vs Li exposure time. The intensity increases linearly with Li exposure time when deposition time is less than 55 min. After 115 min the intensity tends to saturate.

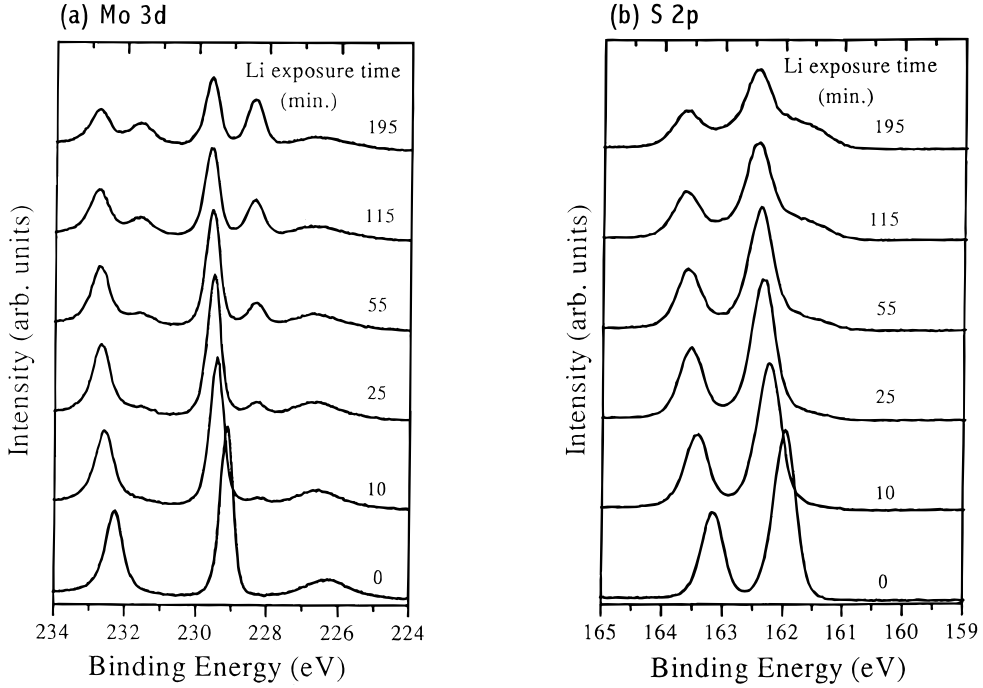


**Figure 3.** The effect of Li deposition on $MoS_2$ core levels. (a) Mo 3d and (b) S 2p. In both cases a Li-reduced peak appeares at the lower binding energy side, and the bulklike peaks all shift to higher binding energy. Notice that the S 2p reduced peaks (fwhm 0.96 eV) are broader than the Mo 3d reduced peaks (fwhm 0.55 eV).

out in the sample treatment chamber and subsequent higher $O_2$ exposure up to $5 \times 10^8$ L ($P_{O_2} = 0.75$ Torr for 30 s and then 10 min) in the sample fast entry chamber. The binding energies in the XPS spectra were calibrated using the position of the Ag $3d_{5/2}$ core line at 368.25 eV, measured using a polycrystalline silver sample (Alfa AESAR).

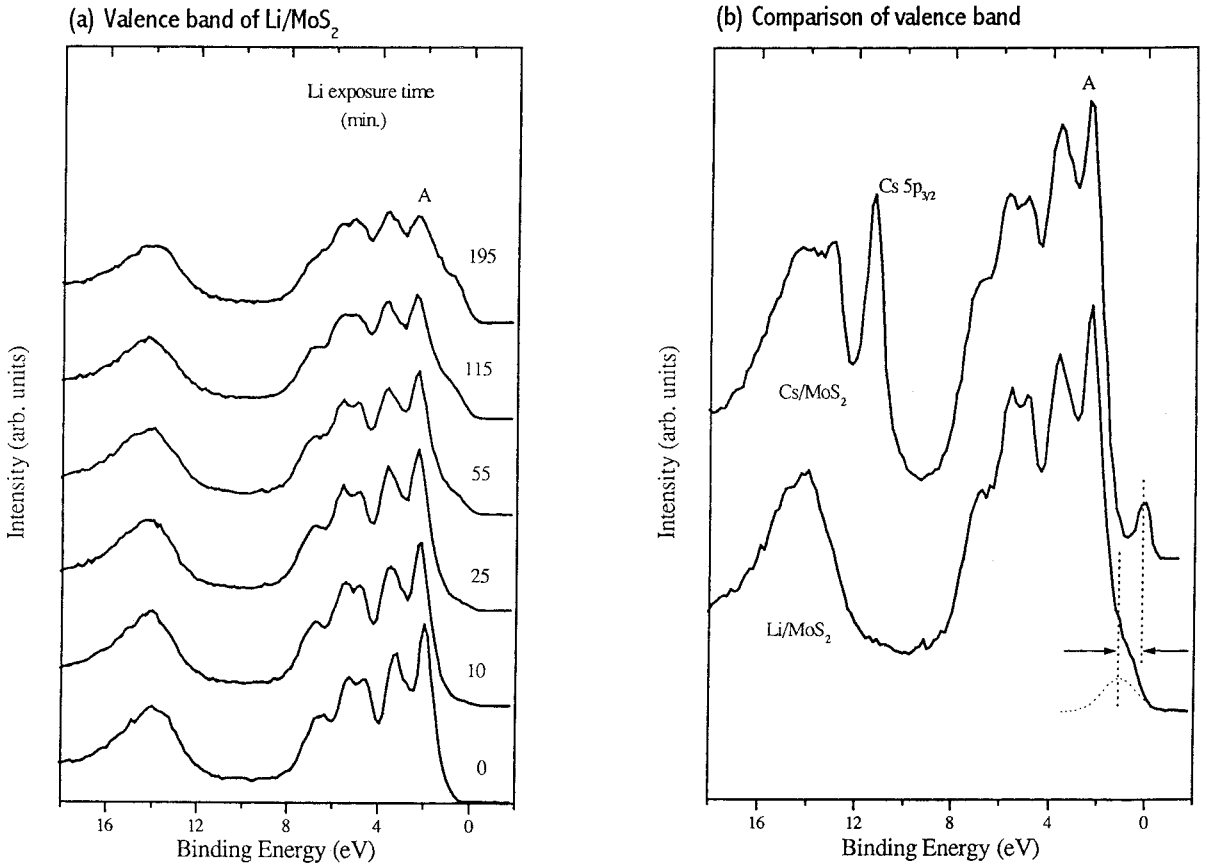


**Figure 4.** The effects of Li deposition on $MoS_2$ valence band. (a) Valence band changes as Li deposition time increase. (b) Comparison of the Li and Cs effect on $MoS_2$ valence band. The new density of state on $Cs/MoS_2$ is narrow (fwhm $\leq$ 0.45 eV) and clearly separated from the top of valence band. The new density of state on $Li/MoS_2$ is broad (fwhm $\approx$ 1.5 eV) and closer to the top of valence band.

**TABLE 1: Binding Energies and Relative Binding Energy Shifts (in Parentheses) (in eV) of the Mo $3d_{5/2}$, S $2p_{3/2}$, and Li 1s Core Levels, Top of Valence Band (VB A peak), and $e^-/MoS_2$**

| | Li exposure time (min) | | | | | |
|---|---|---|---|---|---|---|
| | 0 | 10 | 25 | 55 | 115 | 195 |
| Mo $3d_{5/2}$ bulklike | 229.11 | 229.41 | 229.51 | 229.55 | 229.59 | 229.60 |
| | (0.00) | (0.30) | (0.41) | (0.44) | (0.48) | (0.49) |
| Mo $3d_{5/2}$ reduced | | 228.27 | 228.30 | 228.36 | 228.38 | 228.39 |
| | | (0.00) | (0.03) | (0.09) | (0.11) | (0.12) |
| S $2p_{3/2}$ bulklike | 161.96 | 162.25 | 162.35 | 162.39 | 162.44 | 162.45 |
| | (0.00) | (0.29) | (0.39) | (0.43) | (0.48) | (0.49) |
| S $2p_{3/2}$ reduced | | 161.57 | 161.58 | 161.61 | 161.68 | 161.69 |
| | | (0.00) | (0.01) | (0.04) | (0.11) | (0.12) |
| Li 1s | | 55.69 | 55.73 | 55.78 | 55.79 | 55.82 |
| | | (0.00) | (0.04) | (0.09) | (0.10) | (0.13) |
| VB A peak | 1.95 | 2.18 | 2.27 | 2.28 | 2.37 | 2.34 |
| | (0.00) | (0.23) | (0.32) | (0.33) | (0.42) | (0.39) |
| $e^-/MoS_2$ | | 0.960 | 0.96 | 0.96 | 1.05 | 0.96 |
| | | (0.00) | (0.00) | (0.00) | (0.09) | (0.00) |

## Results

**1. Adsorption of Li on $MoS_2$ (0002).** The presence of Li atoms on $MoS_2$ (0002) was monitored by the Li 1s core level signal (Figure 2a). Throughout the Li deposition, no significant changes in binding energies and peak shapes of the Li 1s core level were observed. The binding energy of the Li 1s level remained nearly constant at 55.8 eV, and its full width at half-maximum (fwhm) was ca. 0.7 eV. After the total 195 min of Li evaporation, the intensity of the Li 1s core level indicated near-saturation (Figure 2b). The effect of Li adsorption on the Mo 3d and S 2p core levels is shown in Figure 3. Before Li deposition, the bare $MoS_2$ (0002) surface exhibited well-separated spin−orbit splittings for the Mo 3d and S 2p core levels as previously reported.[14] The initial 10 min of Li evaporation resulted in new peaks on the lower binding energy side of both the Mo 3d and S 2p core level spectra. The lower binding energy component of the Mo $3d_{5/2}$ peak appeared at 228.27 eV, shifted by 1.14 eV from its bulk component. Likewise, the lower binding energy component of the S $2p_{3/2}$ level appeared at 161.57 eV, which is shifted by 0.68 eV from its bulk core level. In addition, the positions of the bulk peaks in the Mo 3d and S 2p core level spectra were shifted to higher binding energies by ca. 0.3 eV for both core levels. Upon further deposition of Li, the lower binding energy components of the Mo 3d and S 2p peaks continued to grow, whereas the intensities of the bulk components steadily decreased.

Figure 4 shows the effect of Li deposition on the valence band region of $MoS_2$. After 10 min of Li deposition, the VB

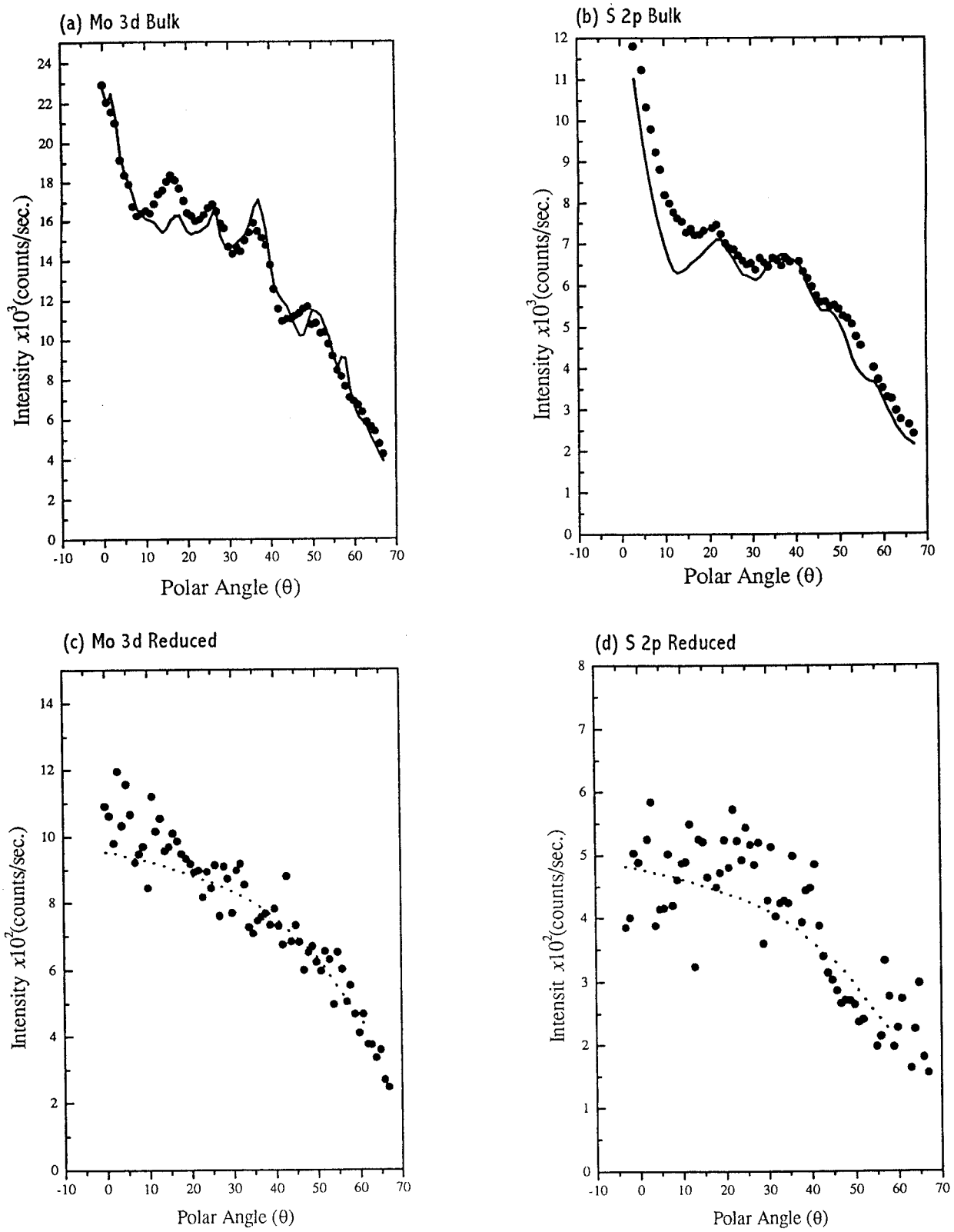


**Figure 5.** ARXPS along $\phi = 60°$. (a) bulklike Mo $3d_{5/2}$ (BE 229.55 eV) with 2H−$MoS_2$ SSC simulation. (b) bulk S $2p_{3/2}$ (BE 162.39 eV) with 2H−$MoS_2$ SSC simulation. (c) Li reduced Mo $3d_{5/2}$ (BE 228.36 eV). Dotted line is the inelastic background scattering with a Li layer of 12 Å fitting from eq 1. (d) Li-reduced S $2p_{3/2}$ (BE 161.61 eV). The dotted line is the inelastic background scattering with a Li layer of 12 Å fitting from eq 1.

XPS spectra displayed an extra density of states at binding energy of 0.96 eV, which is 1.22 eV above the VB peak A. Also, as observed in the core levels, the initial 10 min of Li deposition caused the entire VB spectrum to shift toward higher binding energy by 0.23 eV. The intensity of the new peak above the $MoS_2$ valence band gradually increased as more Li atoms were adsorbed onto the $MoS_2$ basal plane. The binding energies of the most intense peak near the top of VB (peak $A^{12-14}$) as well as the Mo and S core levels are summarized in Table 1 as a function of Li evaporation time.

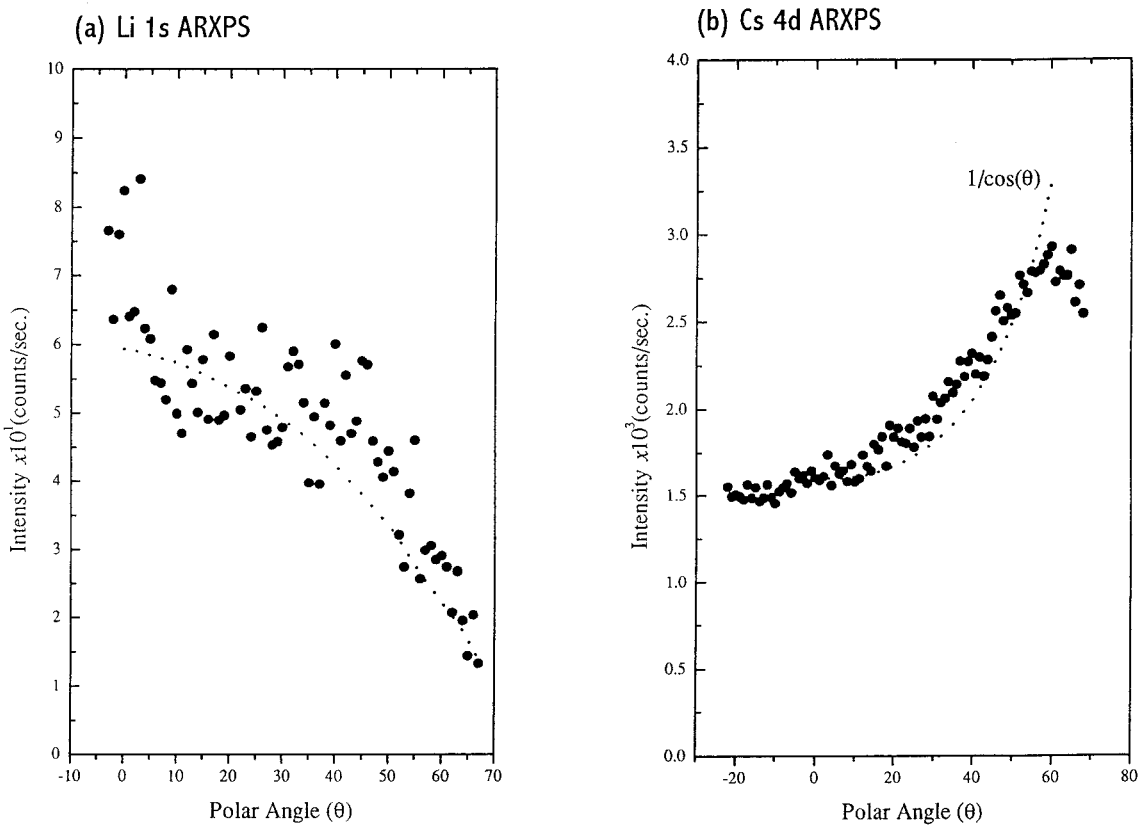


**Figure 6.** (a) Li 1s ARXPS along $\phi = 60°$. The dotted line is the inelastic background scattering with a Li layer of 12 Å fitting from eq 1. (b) Cs 4d ARXPS from ref 13. The dotted line shows the $1/\cos(\theta)$ polar angle dependence.

**2. X-ray Photoelectron Diffraction (XPD) Data.** Figure 5 shows the intensity variation of the Mo $3d_{5/2}$ and S 2p core levels as a function of polar angle $\theta$ along the $\langle 10\bar{1}0 \rangle$ azimuth after 40 min of Li evaporation on $MoS_2$. The intensities of the bulk and the lower binding energy components were calculated by first fitting each component with a Voigt function on a linear background, then integrating the peak area under each decomposed peak. The bulk component of the Mo $3d_{5/2}$ level (Figure 5a) displays a pronounced XPD pattern, dominated by strong forward peaks at 0°, 16°, 26°, 36°, and 49°. Similarly, the bulk component of the S 2p core level shows forward focusing maxima at 0°, 21°, 37°, and 49° (Figure 5b). In a sharp contrast, the Li -reacted Mo and S components at the lower binding energy (parts c and d of Figure 5) display very scattered intensity profile without any easily discernible photoelectron intensity maxima. The polar angle scan of the Li 1s core level also shows quite scattered ARXPS data points (Figure 6a). This behavior is in a sharp contrast with that of the Cs overlayer (Figure 6b).

**3. Reaction of Li/$MoS_2$(0002) with Molecular Oxygen.** The Li-covered $MoS_2$(0002) surface (after the total 195 min of Li evaporation) was exposed to $O_2$ at room temperature. The oxygen partial pressure of $1 \times 10^{-6}$ Torr for 30 min gives the initial exposure of 1800 L. The resulting XPS spectrum shows nearly uniform binding energy shifts of all electronic levels by ca. 0.3 eV toward lower binding energy (Figure 7). Upon initial oxygen exposure, the intensity of the Li-reacted lower binding energy components of the Mo 3d and S 2p core levels decreased significantly more than those of the bulk components. With further exposure at much higher oxygen partial pressure ($P_{O_2} = 0.75$ Torr), the intensity of the lower binding energy components continued to decrease compared to the bulk components (XPS spectra ii−iv in Figure 7). Similarly, as in the core levels, the extra density of states above the $MoS_2$ VB peak A showed a gradual decrease in intensity with increasing $O_2$ exposure. In Figure 8, the corresponding O 1s core level spectra after various $O_2$ exposure are presented. The initial exposure to the low oxygen partial pressure $P_{O_2} = 1 \times 10^{-6}$ Torr gave rise to a strong peak centered at 531.57 eV. After the subsequent oxygen exposures at much higher $O_2$ partial pressure, the O 1s peak further increased, but also a small satellite peak at 528.66 eV was observed.

## Discussion

**1. Stoichiometry and Morphology of the Li/$MoS_2$(0002) Surface Region.** The Li-covered $MoS_2$(0002) surfaces do not exhibit any new LEED spots other than a $(1 \times 1)$ pattern, indicating no long-range ordered Li overlayer or Li-induced surface structure at all Li coverages. Because of this lack of long-range order, the amount of the Li atoms deposited onto the $MoS_2$ basal plane is estimated by comparing the Li 1s intensity with that of the Mo 3d and S 2p levels from a bare $MoS_2$(0002) surface after correcting for the photoionization cross sections.[22] The atomic ratio of Li to Mo after the first 10 min evaporation is 0.10 and continues to increase to 0.62 after the 195 min of Li exposure (Table 2). Considering the fact that XPS probes clean $MoS_2$(0002) to several atomic layers,[12] the measured value after the 195 min of Li deposition points to the formation of multilayer Li. Further information regarding the spatial distribution of the deposited Li atoms can be obtained from ARXPS data of the Li 1s level. The smoothly varying angular profile with large intensity attenuation at higher polar angles (Figure 6a) is in sharp contrast to the polar angle dependence of the photoelectron intensity expected from a thin film on a substrate, for example, the increase in the photoelectron intensity at larger polar angles following approximately

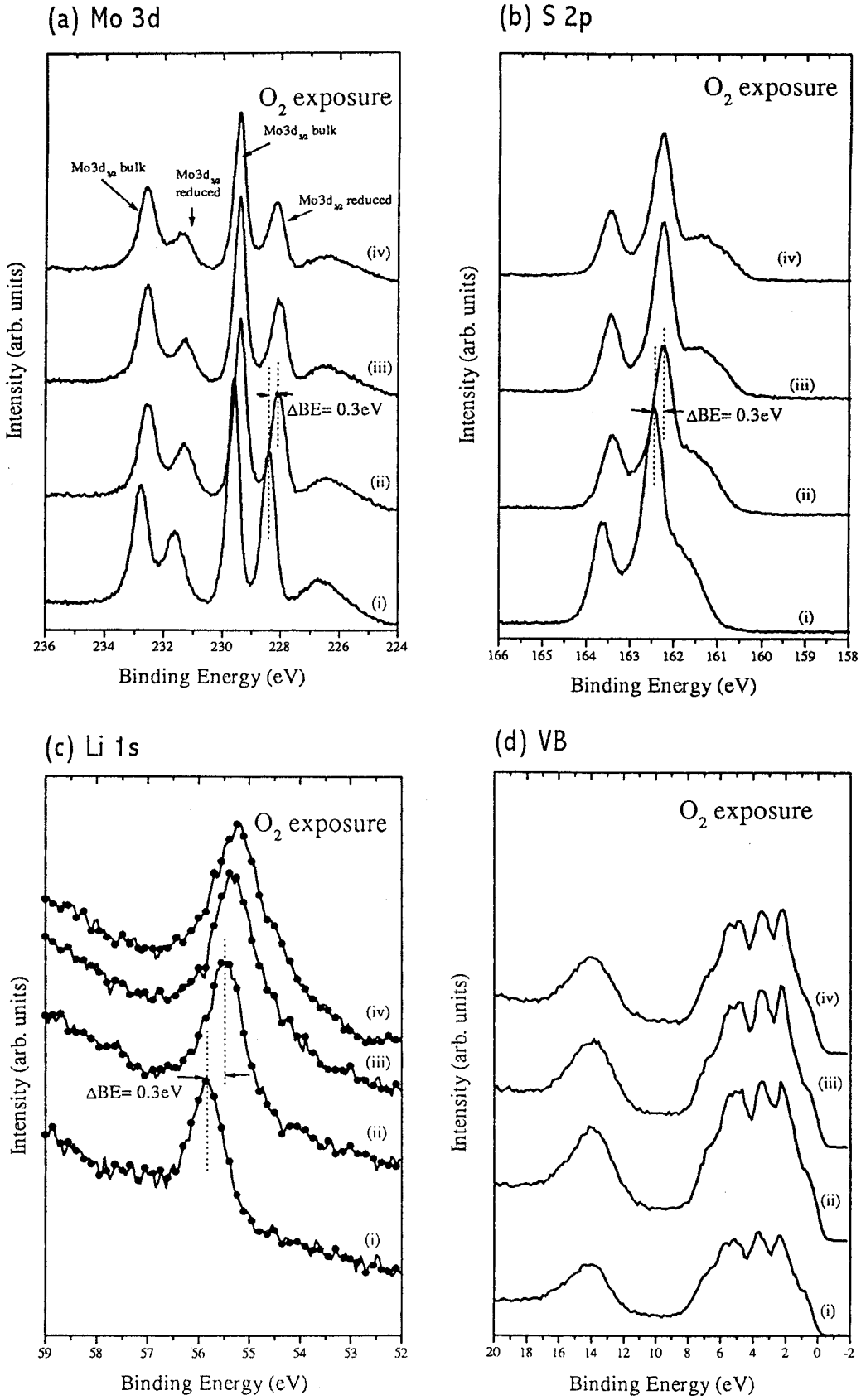


**Figure 7.** $O_2$ exposure effect on (a) Mo 3d, (b) S 2p, (c) Li 1s, and (d) valence band. The $O_2$ exposures are (i) 0 L, before $O_2$ exposure; (ii) $1.8 \times 10^3$ L, 30 min $1.0 \times 10^{-6}$ Torr of $O_2$ exposure; (iii) $2.25 \times 10^7$ L, 30 s 0.75 Torr of $O_2$ exposure; (iv) $5.0 \times 10^8$ L, 10 min 0.75 Torr of $O_2$ exposure.

$1/\cos\theta$ dependence as observed with $Cs/MoS_2(0002)$[13] (Figure 6b), CO/Pd(100), $C_2Cl_4$/Pd(100),[23] and pentamethylcyclopentasiloxane/Pd(100).[24] Instead, the polar angle dependence of the Li 1s core level is quite similar to the background intensity profiles observed in the Mo 3d and S 2p ARXPS (parts c and d of Figure 5), suggesting that the deposited Li atoms are

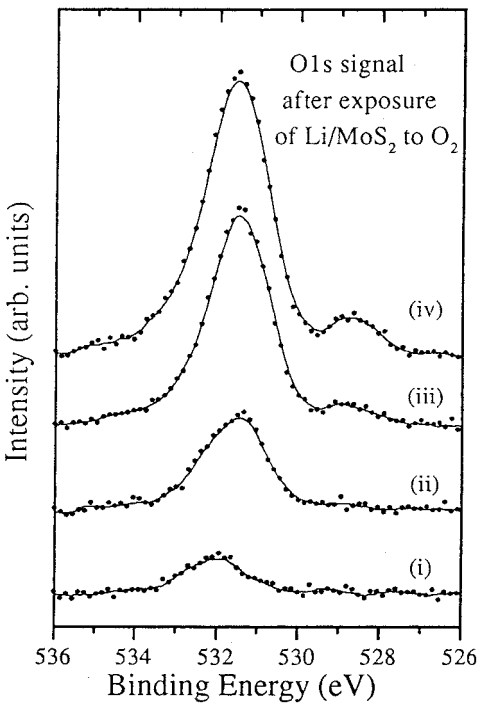


**Figure 8.** $O_2$ exposure effect on the O 1s peak.:(i) 0 L, before $O_2$ exposure; (ii) $1.8 \times 10^3$ L, 30 min $1.0 \times 10^{-6}$ Torr of $O_2$ exposure; (iii) $2.25 \times 10^7$ L, 30 s 0.75 Torr of $O_2$ exposure; (iv) $5.0 \times 10^8$ L, 10 min 0.75 Torr of $O_2$ exposure.

distributed over a relatively thick "layer". In addition, the measured value of 55.8 eV for the Li 1s binding energy is close to 55.6 eV reported for $Li_2O$,[25] but it is much larger than the binding energy of metallic Li, 54.7 eV.[26] Therefore, the deposited Li is most likely inside the $MoS_2$ structure rather than as a metallic multilayer Li on the $MoS_2$ basal plane. The effective thickness of the Li layer can be quantitatively estimated using a semiempirical relation of the photoelectron intensity attenuation due to inelastic scattering,[27]

$$I(\theta) = I_0 \lambda R(\theta) \exp(-z_s/\lambda \cos\theta)[1 - \exp(-z_0/\lambda \cos\theta)] \quad (1)$$

where $I_0$ is the unattenuated intensity, $\lambda$ the inelastic electron mean free path,[28] $R(\theta)$ the instrument response function, $z_s$ the thickness of a screening layer, and $z_0$ the thickness of the photoemission layer. With the value of $\lambda$ equal to 37 Å,[29] eq 1 yields the value for the nominal thickness of the Li layer ca. 12 Å, equivalent to about 2 $MoS_2$ layers.

One of the most striking observations in the Li/$MoS_2$(0002) system is the presence of large intensity lower binding energy components observed in both the Mo 3d and S 2p regions (Figure 2). The measured binding energies of the new satellites, 228.27 eV for Mo $3d_{5/2}$ and 161.57 eV for S $2p_{3/2}$, are close to (albeit not identical with) the literature values of 228.0 eV for Mo metal[30] and 161.8 eV for $Na_2S$,[31] suggesting reduction of $MoS_2$ by Li. This BE shifts are consistent with a previous result which reported that the $Li^7$ wide-line NMR spectrum of Li-intercalated $MoS_2$ was similar to that from pure $Li_2S$.[32] A similar reduction of 2H−$WS_2$ to $Li_2S$ and metallic W by Li deposited at room temperature was also reported.[33] However, the currently determined experimental stoichiometry between Li and the reduced Mo is well below the expected 4:1 for full reduction to Mo metal except after the initial Li coverage (Table 2).[34] Therefore, the observed results of the BE shifts and stoichiometry between Li and the reacted Mo imply a partial reduction by adsorbed Li to form $Li_xMoS_2$ ($x \approx 2$) rather than a complete reduction via the reaction $4Li + MoS_2 \rightarrow 2(Li_2S) + Mo$. The atomic ratio of Li to the reduced Mo is found to be almost exactly 2:1 at high Li coverages, thus it could suggest a possible formation of $Li_2MoS_2$. The lower valence state Mo(II) in $Li_2$-$MoS_2$ is consistent with the observed Mo$3d_{5/2}$ binding energies of the "reduced" Mo species (Table 1) and is analogous to the known existing sulfide Mo(II)S.[35]

In terms of structural changes probed by ARXPS, Li deposition leaves the unreduced portion of $MoS_2$ intact, while the reduced portion is converted to an amorphous compound of stoichiometry Li/Mo = 2:1 as demonstrated in Table 1. The *bulk* Mo 3d and S 2p ARXPS data show typical XPD patterns of a single-crystal $MoS_2$(0002), which are dominated by pronounced forward-focusing maxima.[12] For more quantitative analysis, a single scattering cluster (SSC) model[17] was presently used to simulate the observed the XPD patterns of the bulk Mo 3d and S 2p core levels. The bulk values of the lattice parameters for 2H−$MoS_2$ structure,[1] $a = 3.16$ Å and $c = 12.30$ Å, were chosen in the SSC simulations. The cluster size chosen for the SSC calculations was $7 \times 7 \times 4$ ($N_a \times N_b \times N_c$), where $N_a$, $N_b$, and $N_c$ are the numbers of the $MoS_2$ molecular units along the Bravais lattice vectors **a**, **b**, and **c**. The scattering calculation was carried out in the plane-wave approximation, and the calculated ARXPS data points were further averaged to simulate angle-averaging due to the finite acceptance cone angle of the Scienta ESCA 300 detector ($\Delta\theta \approx 4°$).[13] Also included is the smoothly varying background intensity profile for a polar angle scan due to inelastic scattering using eq 1. The positions and intensities of the observed diffraction maxima are in excellent agreement with the SSC theory as shown in parts a and b of Figure 5. On the contrary, the ARXPS data of the *reduced* Mo 3d and S 2p core levels exhibit very scattered ARXPS data points without any forward focusing maxima for the reduced Mo 3d and S 2p core levels, indicating that the reduced Mo and S layers no longer possess well-defined crystallinity observed from clean $MoS_2$(0002). This result is consistent with a substantial reactive reconstruction of the crystal lattice after the Li intercalation, previously reported in a number of X-ray diffraction experiments.[5,36] The smoothly varying angular profile with large intensity attenuation at higher polar angles is similar to that from the Li 1s ARXPS data implying the extended "layers" of the reduced $MoS_2$. The best fit of data in Figure 6a to eq 1 yields the value of about 12 Å for the nominal thickness $z_0$ using the value of $\lambda$ equal to 35 Å.[37]

**2. Valence Bands in Li/$MoS_2$ and Cs/$MoS_2$.** Comparing the present Li/$MoS_2$ composite with the previously examined Cs/$MoS_2$, one easily notices that the BE and the fwhm of the supravalence electron peak above the $MoS_2$ VB maximum are substantially different (Figure 4b). The binding energy of the supravalence electron peak in Li/$MoS_2$ is only 1.22 eV above the $MoS_2$ VB A peak, which places the new density of states at ca. 0.3 eV above the $MoS_2$ VB maximum (VBM), well below the $MoS_2$ conduction band minimum (CBM).[14] Moreover, the measured value of ca. 1.5 eV for the fwhm of the supravalence electron peak in Li/$MoS_2$ is much larger than 0.45 eV in Cs/$MoS_2$, which is characteristic of narrow *d* bands. The clear contrast observed in the valence bands strongly suggests that the electron transfer reaction in Li/$MoS_2$ is not a simple process that can be understood on the basis of a rigid-band model as in Cs/$MoS_2$. Instead, the observed supravalence electron density in the Li/$MoS_2$ valence band originates from the reduction of $MoS_2$ forming $Li_2S\cdots$Mo(II)S and subsequent degradation of the $MoS_2$ crystallinity. The results further imply that the electron transfer from alkali metal to $MoS_2$ alone does not induce the

**TABLE 2: Core Level Intensity as a Function of Li Exposure Time**

| Li exposure time (min) | Li 1s ($\sigma = 0.0568$)[a] (counts/s) | Mo $3d_{5/2}$ ($\sigma = 5.62$)* bulklike | Mo $3d_{5/2}$ ($\sigma = 5.62$)* reduced | S $2p_{3/2}$ ($\sigma = 1.11$)* bulklike | S $2p_{3/2}$ ($\sigma = 1.11$)* reduced | S/Mo (reduced) | S/Mo (bulklike) | Li/Mo (clean) |
|---|---|---|---|---|---|---|---|---|
| 0 | 0 | 8.620 | 0 | 4.293 | 0 | | 2.52 | |
| 10 | 0.0088 | 8.500 | 0.206 | 4.174 | 0.092 | 2.26 | 2.48 | 0.101 |
| 25 | 0.0162 | 7.908 | 0.610 | 3.968 | 0.243 | 2.01 | 2.54 | 0.186 |
| 55 | 0.0241 | 6.712 | 1.219 | 3.472 | 0.457 | 1.90 | 2.62 | 0.277 |
| 115 | 0.0454 | 5.383 | 2.016 | 2.848 | 0.812 | 2.03 | 2.68 | 0.521 |
| 195 | 0.0543 | 4.210 | 2.887 | 2.168 | 1.096 | 1.92 | 2.61 | 0.623 |

[a] The values of the photoionization cross sections $\sigma$ are taken from ref 21 and are given in the unit of barn.

**TABLE 3: Core Level Intensity as a Function of $O_2$ Exposure**

| | Mo $3d_{5/2}$ bulklike | Mo $3d_{5/2}$ reduced | S $2p_{3/2}$ bulklike | S $2p_{3/2}$ reduced | Li 1s | O 1s | |
|---|---|---|---|---|---|---|---|
| (a) 195 min. Li exposure[a] | $4.369 \times 10^3$ | $2.708 \times 10^3$ | $2.178 \times 10^3$ | $1.096 \times 10^3$ | $5.435 \times 10^1$ | $4.034 \times 10^2$ | 0 |
| (b) $O_2$ 30 min $10^{-6}$ torr | $1.054 \times 10^4$ | $5.981 \times 10^3$ | $4.943 \times 10^3$ | $2.073 \times 10^3$ | $1.624 \times 10^2$ | $2.778 \times 10^3$ | 0 |
| (c) $O_2$ 30 sec. $0.75 \times 10^{-3}$ torr | $1.008 \times 10^4$ | $5.075 \times 10^3$ | $4.566 \times 10^3$ | $2.718 \times 10^3$ | $2.126 \times 10^2$ | $6.489 \times 10^3$ | $1.698 \times 10^2$ |
| (d) $O_2$ 10 min $0.75 \times 10^{-3}$ torr | $9.017 \times 10^3$ | $4.884 \times 10^3$ | $3.774 \times 10^3$ | $2.054 \times 10^3$ | $2.540 \times 10^2$ | $8.492 \times 10^3$ | $7.522 \times 10^2$ |

[a] The data for this exposure were taken with X-ray power of 2.7 kW, the rest with 6.8 kW.

proposed phase transition from 1T to 2H structures as suggested by others.[5,15]

The exposure of the Li-covered $MoS_2$(0002) surface to $O_2$ reoxidizes the Li-reduced $MoS_2$(0002) surface, as evidenced by the partial reversal of binding energy shifts of the Mo 3d and S 2p levels (Figure 7). With increasing oxygen exposure, the amount of the reduced Mo and S species decreases much faster than the bulk counterparts (Table 3). It is worth noting that the Li 1s core level intensity also increases with the increasing $O_2$ exposure, suggesting that the oxygen adsorption "pulls out" the subsurface Li atoms back to the outer surface of the basal plane. This observation is consistent with previous reports that X-ray diffraction patterns of alkali-doped $MoS_2$ revert to that of pure $MoS_2$ under the presence of moisture.[3,36,38] The O 1s core level spectra indicate that most of the reoxidation proceeds to form a peroxidic $Li_2O_2$ species, evidenced by the O 1s binding energy position at 531.57 eV.[39,40] At higher oxygen partial pressure, a small O 1s satellite at 528.66 eV implies the presence of additional small amount of $Li_2O$. However, as indicated by the Mo 3d and S 2p core levels and the VB XPS spectra (Figure 7), a substantial amount of the Li-reduced $MoS_2$ remains unoxidized even after the high-pressure $O_2$ exposure.

## Conclusions

In this study, we found HRXPS evidence that in situ deposited Li reacts with the $MoS_2$(0002) surface closely represented as $2Li + MoS_2 \rightarrow Li_2S + Mo(II)S$, possibly forming an amorphous compound $Li_2MoS_2$. The ARXPS data further indicate that the deposited Li together with the reduced $MoS_2$ surface forms a highly disordered surface layer, approximately 12 Å deep into the $MoS_2$ bulk, while keeping the unreduced $MoS_2$ structurally intact. The chemical reduction by Li and subsequent degradation of the crystallinity of Li/$MoS_2$(0002) surface introduce supravalence peak inside the $MoS_2$ band gap, at ca. 0.3 eV above the $MoS_2$ VBM. These findings strongly point to the fact that the reaction between the alkali metal and the chalcogenide in Li/$MoS_2$(0002) is not a simple electron transfer described by the rigid band model, in contrast to that in the Cs/ $MoS_2$(0002) system.

**Acknowledgment.** We are grateful to A. Miller of the Scienta ESCA laboratory for the time allocation and technical assistance. Financial support of the Department of Energy Basic Energy Sciences no. DE-FG02-86ER13580 is also acknowledged.

## References and Notes

(1) Wilson, J. A.; Yoffe, A. D. *Adv. Phys.* **1969**, *18*, 193.
(2) Chen, B.-H.; Eichhorn, B.; Peng, J.-L.; Greene, R. L. *J. Solid State Chem.* **1993**, *103*, 307.
(3) Somoano, R. B.; Hadek, V. J.; Rembaum, A. *J. Chem. Phys.* **1973**, *58*, 697.
(4) Somoano, R. B.; Rembaum, A. *Phys. Rev. Lett.* **1971**, *27*, 402.
(5) Py, M. A.; Haering, R. R. *Can. J. Phys.* **1983**, *61*, 76.
(6) Imanishi, N.; Toyoda, M.; Takeda, Y.; Yamamoto, O. *Solid State Ionics* **1992**, *58*, 333.
(7) Jaegermann, W.; Tributsch, H. *Prog. Surf. Sci.* **1988**, *29*, 1.
(8) Conway, M. M.; Murchison, C. B.; Stevens, R. R. U.S. Patent 4,675,344, June 23, 1987 (assigned to Dow Chemical Co).
(9) Kinkade, N. E. Eur. Patent Appl. 84116467.6 and 84116468.4, Dec. 28, 1984 (assigned to Union Carbide Corporation).
(10) Santiesteban, J. G.; Bogdan, C. E.; Herman, R. G.; Klier, K. *Proceedings of the 9th International Congress of Catalysis* (Calgary); North-Holland Publishing Co.: Amsterdam, 1988; p 561.
(11) Santiesteban, J. G. Ph.D. Thesis, Lehigh University, 1988.
(12) Park, K. T.; Richards-Babb, M.; Freund, M. S.; Weiss, J.; Klier, K. *J. Phys. Chem.* **1996**, *100*, 10739.
(13) Park, K. T.; Richards-Babb, M.; Weiss, J.; Klier, K. *Phys. Rev.* **1996**, *B54*, 5471.
(14) Park, K. T.; Hess, J. S.; Klier, K. *J. Chem. Phys.* **1999**, *111*, 1636.
(15) Papageorgopoulos, C. A.; Jaegermann, W. *Surf. Sci.* **1995**, *338*, 83.
(16) The work functions of $MoS_2$ range from 4.1 to 4.55 to 4.8 eV depending on the methods and sources of measurement (refs 15, 43, and 44, respectively, from Richards-Babb, M. Ph.D. Thesis, Lehigh University, 1989). The work functions of metallic Cs and Li are 1.95 and 2.93 eV, respectively, from CRC Handbook of Chemistry and Physics, 79th ed. (Lide, D. R., Ed.; CRC Press LLC: Boca Raton, 1998; p 12−124) whereas the ionization energies are 3.89 and 5.39 eV for Cs and Li.
(17) Fadley, C. S. *Synchrotron Radiation Research Advances in Surface and Interface Science*; Bachrach, R. Z., Ed.; Plenum: New York, 1990.
(18) Egelhoff, W. F. *CRC Crit. Rev. Solid State Mater. Sci.* **1990**, *16*, 213 and references therein.
(19) *Photoemission in Solids I*; Cardona, M., Ley, L., Eds.; Springer-Verlag: Berlin, 1978.
(20) *SCIENTA ESCA-300 User's Manual*; Scienta: Uppsala. Alternatively, one can obtain a general overview of the spectrometer from: *High-Resolution XPS of Organic Polymers, The Scienta ESCA 300 Database*; Beamson, G., Briggs, D., Ed.; Wiley: Chichester, 1992; pp 3−8.
(21) Park, K. T.; Simmons, G. W.; Klier, K. *Surf. Sci.* **1996**, *367*, 307.
(22) Scofield, J. H. *J. Electron Spectrosc.* **1976**, *8*, 129.
(23) Park, K. T.; Klier, K.; Wang, C. B.; Zhang, W. X. *J. Phys. Chem.* **1997**, *101*, 5420.
(24) Park, K. T.; Herman, R. G.; Klier, K. *Surf. Sci.* **1998**, *417*, L1125.

(25) Contour, J. P.; Salesse, A.; Froment, M.; Garreau, M.; Thevenin, J.; Warin, D. J. *J. Microsc. Spectrosc. Electron.* **1979**, *4*, 483.
(26) Kowalczyk, S. P.; Ley, L.; McFeely, F. R.; Pollak, R. A.; Shirley, D. A. *Phys. Rev.* **1973**, *B8*, 3583.
(27) *Practical Surface Analysis*; Briggs, D., Seah, M. P., Eds.; John Wiley & Sons: Chichester, 1983.
(28) Seah, M. P.; Dench, W. A. *Surf. Interface Anal.* **1979**, *1*, 2.
(29) The semiempirical formular for inorganic compounds given in ref 28 was used with the kinetic energy of the Li 1s photoelectrons $E_k$ equal to 1430 eV.
(30) Wagner, C. D.; Taylor, J. A. *J. Electron. Spectrosc. Relat. Phenom.* **1980**, *20*, 83.
(31) Swartz, W. E.; Wynne, K. J.; Hercules, D. M. *Anal. Chem.* **1971**, *43*, 1884.
(32) Silbernagel, B. G. *Solid State Commun.* **1975**, *17*, 361.
(33) Schellenberger, A.; Jaegermann, W.; Pettenkofer, C.; Kamaratos, M.; Papageorgopoulos, C. A. *Ber. Bunsen-Ges. Phys. Chem.* **1994**, *98*, 833.
(34) The initially large ratio of Li to the reduced Mo is perhaps due to the excess Li on $MoS_2$ surface, and the gradual decrease in the atomic ratio can be explained by the Li diffusion as suggested in ref 15.
(35) Greenwood, N. N.; Earnshaw, A. *Chemistry of the Elements* (Pergamon: Oxford, 1984), p 1186.
(36) Whittingham, M. S.; Gamble, F. R., Jr. *Mater. Res. Bull.* **1975**, *10*, 363.
(37) The semiempirical formula for inorganic compounds given in ref 28 was used with the kinetic energy of the Mo $3d_{5/2}$ equal to 1257 eV.
(38) Whittingham, M. S. *Prog. Solid St. Chem.* **1978**, *12*, 41.
(39) Jupille, J.; Dolle, P.; Besancon, M. *Surf. Sci.* **1992**, *260*, 271.
(40) Hrbek, J.; Wang, Y. W.; Rodriguez, J. A. *Surf. Sci.* **1993**, *296*, 164.